Int. J. Electrochem. Sci., 17 **(2022)** Article Number: 220715, doi: 10.20964/2022.07.17

International Journal of
ELECTROCHEMICAL
SCIENCE
www.electrochemsci.org

Preparation and Electrochemical Sensing Properties of Vanillin Molecularly Imprinted Polymer

Jianlian Liu[1,2,] *Chaojun Du*[1,2], *Shengyun Wang*[2], *Zhaoyang Li*[1,*]

[1] School of Railway Transportation, Hunan Technical College of Railway High-Speed, Hengyang, Hunan, 421002, China
[2] School of Biological and Chemical Engineering, Nanyang Institute of Technology, Nanyang, Henan 473004, China
[*]E-mail: crocodiman2020@163.com

Received: 9 February 2022 / *Accepted:* 1 April 2022 / *Published:* 6 June 2022

Molecularly imprinted polymers (MIP), as functional polymers, have the ability to selectively recognize template molecules and have been widely used in various fields. Vanillin (VAN), an important taste component in food, can be found in the seeds of the tropical flower orchid. Based on the benefits of MIP and membrane separation technology, vanillin imprinted blend membrane was successfully created utilizing VAN as template molecule. MIP was employed for electrode modification to perform highly sensitive detection of VAN. The mechanics of imprinting, elution and electrode regeneration were explored. The adsorption behavior of vanillin on electrode was examined. Under optimal conditions, the MIP based electrochemical sensor can perform linear detection of VAN at 1×10^{-11}-1×10^{-4} M. The detection limit is 5×10^{-12} M.

Keywords: Vanillin; Molecularly imprinted polymer; Electrochemical sensor; Specific recognition; Electrochemical behavior

1. INTRODUCTION

Numerous chemistry disciplines have contributed to the development of molecular imprinting technology (MIP). This method allows for the selective identification of certain compounds via polymers [1,2]. MIP's origins date all the way back to the 1940s and 1950s. At the period, when people were examining the mechanism of antigen and antibody synthesis, Pauling, who had received the Nobel Prize in chemistry at the time, first stated the template theory of antibody formation [3]. He stressed that once antigenic material enters the body, it proceeds to construct itself using the protein or polypeptide chain as a template for bending and folding [4]. Although numerous studies undertaken by numerous individuals later demonstrated Pauling's idea to be erroneous, his view had a profound effect on

subsequent generations' research of MIP [5]. MIP is an ingenious technique that relies on memory replication. Bonding is accomplished through the interaction of two or more molecules. During the production of complex, blocked polymers, a certain degree of integrity is maintained [6–8]. MIP's macromolecular skeleton possesses molecular selective recognition capability. When the target molecule (template molecule) comes into contact with the functional monomer, several binding sites are generated, and this relationship is reinforced through further polymerization [9–14]. Thus, after the template molecules are removed, the three-dimensional holes in MIP not only have a spatial structure similar to the template molecules, but also contain functional groups capable of interacting with them [15,16].

Vanillin (VAN) is a significant food flavoring agent that is frequently utilized in a variety of dishes to enhance the flavor of milk. Additionally, it is a key component of epilepsy medications. VAN in high dosages can produce headaches, nausea, vomiting, dyspnea, and even liver and renal damage [17,18]. As a result, the Ministry of Health has imposed stringent restrictions on the amount of VAN permitted in infant formula and cereals. VAN can be determined using a variety of techniques, including high performance liquid chromatography (HPLC) and thin layer chromatography (TLC) [19,20]. Due to VAN's electrochemical activity, it may be determined in principle using an electrochemical technique. However, VAN exhibits weak electrochemical activity, and the oxidation products readily adhere on the electrode surface, resulting in electrode contamination [21–27]. As a result, a modified electrode is required for measurement. Due to the difficulty of excluding the influence of common coexisting compounds using present methods, a more straightforward, inexpensive, and highly selective method is required. MIP has the ability to selectively adsorb target molecules (template/imprinted molecules) [28–33]. The sensitivity and selectivity of the determination can be increased by employing this highly selective adsorption [34–39]. Following over two decades of research, molecular imprinting technology has gained widespread adoption.

VAN molecularly imprinted polymer was synthesized in this work using VAN as the template molecule, -methylphenenic acid (MAA) as the functional monomer, dimethyl sulphoxide (DMSO) as the solvent, ethylene glycol dimethylpropylester (EGDMA) as the crosslinking agent, and azodiethylbutylamine (AIBN) as the initiator. The experiment investigated the dosage of functional monomer, the imprinting mechanism, and the micromorphology of imprinted polymer, as well as the optimal manufacturing process. The products were assessed using a UV spectrophotometer and a Fourier transform infrared spectrometer, as well as the polymer's adsorption properties. Following that, a molecularly imprinted polymer membrane modified electrode was created by coupling molecular imprinting with chemical modification. The electrode made in this manner is suitable for determining VAN in solution and has excellent stability and selectivity.

2. EXPERIMENTAL

VAN, MAA, EGDMA, AIBN and DMSO were all purchased from Tianjin Regent Chemicals Co., Ltd. All of the other reagents were of analytical quality and were utilized without any additional purification or purifying steps. The electrolyte utilized throughout the experiment was phosphate-buffered saline (PBS).

LK98B ii Microcomputer Electrochemical Analysis System (Tianjin Lanlike Company). Three electrodes were used for electrochemical detection: glassy carbon electrode working electrode, saturated calomel electrode (SCE) as reference electrode, platinum wire electrode (PT-Wire) as auxiliary electrode. UV-204 dual-wavelength UV-visible spectrophotometer (Shimadzu) was used to record UV-VIS spectra. TENSOR37(BRUKER) was used to determine FTIR spectra.

Weigh 0. 1522 g (1 mM) template molecule VAN and dispersed into 800 mL DMSO. 0.34 mL (4 mM) functional monomer MAA was added into the solution and sonicated at room temperature for 1h to fully interact with the functional monomer and template molecules. After the mixture was evenly mixed, a certain amount of crosslinking agent EGDMA and an appropriate amount of initiator AIBN were added, and nitrogen was injected for 30 min before sealing. Under the protection of nitrogen, the solution was placed in a collector constant temperature heating magnetic stirring device, stirring at 50°C constant temperature and constant speed, and the polymerization was initiated by heat for 24 h. After cooling to room temperature, the reactants were centrifuged to obtain imprinted polymer microspheres (MIPs). The synthesized polymer microspheres were put into a Soxhlet extractor and extracted with methanol/acetic acid (V/V = 9/1) to elute the imprinted molecules until VAN in the reflux solution could not be detected by UV spectrum. It was then washed several times with methanol to remove excess acetic acid, and finally dried in a vacuum oven at 60°C for later use. GCE was cleaned and dried in the open air. 5 μL MIPs solution (1 mg/mL) was applied to the surface of this GCE, which was then allowed to dry. Blank imprinted polymer microspheres (NIPs) were synthesized without the addition of VAN, and other experiments were the same.

Adsorption kinetics of molecularly imprinted polymers: Weigh 10 equal quantities of MIP and NIP 10 mg each, and add 5mL of van-DMSO solution with 2 mM concentration to each. The solution was sonicated at room temperature for a certain time (15,30,45,60,75,90,120,150,180,240 min), and the mixture at each time was immediately transferred to the separator for centrifugation for 15 min. Then, 1 mL supernatant was removed and diluted to 5 mL with DMSO. The absorbance of the solution was measured at the maximum absorption wavelength with DMSO as a reference by UV spectrophotometer. The equilibrium concentration of template molecule VAN was determined according to the variation of VAN concentration in solution before and after adsorption.

3. RESULTS AND DISCUSSION

The imprinted molecule's VAN concentration was maintained constant, while the functional monomer MAA concentration was steadily increased. As illustrated in Figure 1, a series of UV absorption spectra was measured. As can be seen, the absorbance decreases as the number of functional monomers increases, indicating that the force between functional monomer MAA and imprinted molecule VAN is increased [40,41]. By comparing the absorbance at the maximum absorption wavelength shown in the figure, we discovered that when the molar ratio of imprinted molecule to functional monomer exceeded 1:4, the dosage dimension of functional monomer continued to grow, and the change in absorption peak intensity was not as obvious. This implies that increasing the proportion of functional monomers can facilitate self-assembly between imprinted molecules and functional

monomers within a limited range, but that increasing the dosage does not necessarily improve the process [42–44]. This is because when the concentration of functional monomer is too high, unassembled functional monomer residues are easily formed. As a result, the number of non-selective binding sites in MIP will increase while the number of unique selective recognition sites would decrease. Second, if the amount of functional monomer is excessive, self-association is more likely to occur, impairing the accuracy with which the identification site is fixed and produced, and increasing the mass transfer resistance of adsorption in MIP [45]. As a result, in order to maximize the recognition effectiveness and stability of the synthesized MIP, 1:4 is chosen as the optimal mole ratio in the experiment.

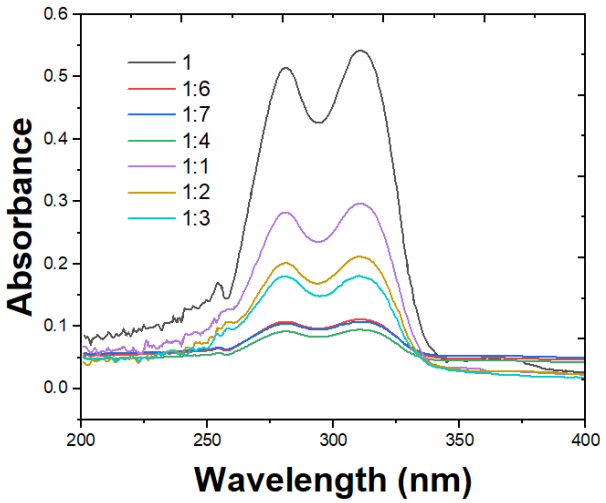

Figure 1. UV-vis spectra of VAN and MAA with ratios of 1:0, 1:1, 1:2, 1:3, 1:4, 1:5, 1:6 and 1:7 in DMSO.

The functional groups and chemical bonds of the tested substance can be determined according to the position, intensity and shape of the absorption peaks in the infrared spectrogram. Therefore, the specific functional groups that interact with functional monomers and the imprinting mechanism of MIP synthesis can be further learned by analyzing the FTIR spectra of each polymer [46]. Figure 2 shows the ir spectra of MIP before elution, target molecule VAN, MIP and NlP after elution. In the infrared spectrum of VAN, the stretching vibration absorption peak of OH is about 3200cm^{-1} [47]. The stretching vibration absorption peak of aldehyde group is about 1670 cm^{-1}, while the bending vibration absorption peak of phenolic hydroxyl group is about 1260 cm^{-1}. In the FTIR spectrum of MIP before elution, it can be seen that the stretching vibration absorption peak band of the original template molecule VAN at 1670 cm^{-1} moves to the high wave number segment to about 1730 cm^{-1} [48,49]. This indicates that the C=O bond in VAN molecule may form a binding site of ammonia bond with the ammonia atom on COOH in MAA. However, the stretching vibration absorption peak blue of OH bond at 3200 cm^{-1} on original VAN shifted to about 3400 cm^{-1} [50]. This indicates that strong intermolecular force has been generated between VAN and MAA, and it proves that there may be strong ammonia bonding between -OH in VAN and C=O in MAA. In addition, the infrared spectral characteristics of the elution MIP and

NIP are basically the same, indicating that the template molecule VAN in MIP is eluded, leaving a hole structure matching its functional group [51].

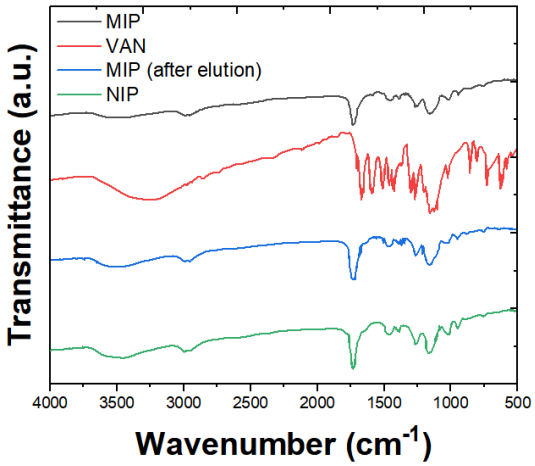

Figure 2. FTIR spectra of MIP, VAN, MIP after elution and NIP.

A critical way for studying the adsorption kinetics of imprinted polymers is to determine their kinetic adsorption curve, which represents the connection between the adsorption quantity Qt (adsorption quantity at a certain point in time) and the time t. The adsorption capacity of the imprinted polymer to the target molecule at various times was examined [52,53], while the polymer mass and starting concentration of the template molecule solution remained constant. MIP and NIP adsorption kinetics are depicted in Figure 3A.

As illustrated in Figure 3A, the adsorption rate increases dramatically with time. Once a given period has passed, the growing rate of adsorption begins to slow, and eventually adsorption tends to equilibrium. This is because, during the earliest stages of adsorption, the surface of MIP contains a large number of holes and cavities compatible with the template molecule structure. MIP utilizes the pore ash and cavity on these surfaces to detect the adsorption imprinted molecule VAN, which results in a reasonably high adsorption rate of MIP on the imprinted molecule at this stage [54]. The effective binding sites between surface pores and cavities gradually decrease as the adsorption process continues. Then the rate of adsorption will decrease. When the adsorption between these surface pores and cavities becomes saturated, the imprinted molecules diffuse into the MIP's deep pores, resulting in a certain mass transfer resistance [55]. As a result, the adsorption rate continues to decrease until equilibrium adsorption occurs. Additionally, THE MIP's adsorption capacity on VAN is much greater than that of the NIP, demonstrating that the MIP has a high capacity for VAN adsorption [56].

Adsorption kinetics can be classified into quasi-first-order and quasi-second-order kinetic models [57]. We fitted the kinetic adsorption data of imprinted microspheres, compared their linear correlation, and determined that the quasi-second-order kinetic model best described the imprinted microspheres' adsorption features (Figure 3B).

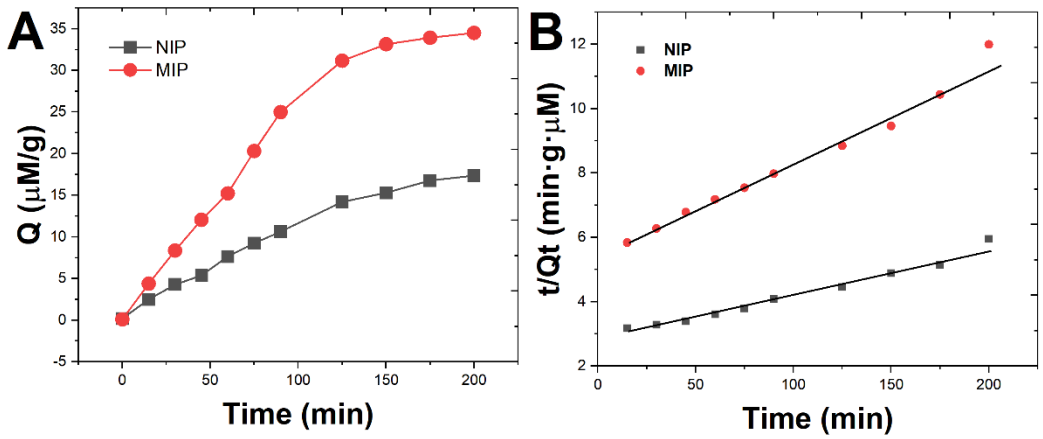

Figure 3. (A) Adsorption dynamic curves and (B) second-order kinetics of MIP and NIP on VAN.

Three electrochemical measurements including cyclic voltammetry (CV), differential pulse voltammetry (DPV) and alternating current impedance (EIS) were used to characterize the electrodes in 5 mM $[Fe(CN)_6]^{3-/4-}$ solution [58,59]. Figure 4A shows CV curves at different polymerization stages. It can be seen from the figure that $[Fe(CN)_6]^{3-/4-}$ probe ions easily undergo redox reactions on the surface of the bare electrode. After modification with MIP and combined with VAN, the current signal decreases. This is because the part of $[Fe(CN)_6]^{3-/4-}$ is prevented from entering the electrode surface by VAN covering [60]. After elution of template molecules in MIP, $[Fe(CN)_6]^{3-/4-}$ can contact the electrode surface through the imprinted cavity, resulting in electrochemical reaction and a slight increase in current [61]. After VAN molecules were recognized, part of the cavity was occupied by template molecules, and the number of $[Fe(CN)_6]^{3-/4-}$ reaching the electrode surface decreased, and the response current intensity decreased.

The DPV curves of electrodes at various phases are shown in Figure 4B. As illustrated in the figure, the current variation of DPV is consistent with the CV variation at various phases, demonstrating the reliability of electrode preparation at various stages [62].

The electrochemical impedance spectroscopy technique has been extensively utilized to analyze charge transport during electrode interface recognition. EIS were obtained in the frequency range of 100 kHz to 0.1 Hz for each stage of electrode modification. The simplified equivalent circuit depicted in Figure 4C is where R_s denotes the electrolyte resistance, C_{dl} is the interface capacitance, R_{ct} denotes the charge transfer resistance, and Z_w denotes the Warburg impedance. The diameter of the high frequency semicircle in the spectrogram corresponds to the redox probe's electron transfer resistance R_{ct} [63]. Following MIP modification on the electrode surface and identification of VAN, the R_{ct} of the charge transfer resistance rose, as did the diameter of the semicircle. This shows that a portion of the redox probe on the electrode surface is blocked by the electrode surface covered by VAN molecules. The impedance value drops when the template molecules are eluted due to the creation of an imprinted molecular cavity on the electrode surface. When the target molecule is detected again, the cavity is filled with VAN molecules, increasing the impedance in the same way that the prior current transformation increased the impedance.

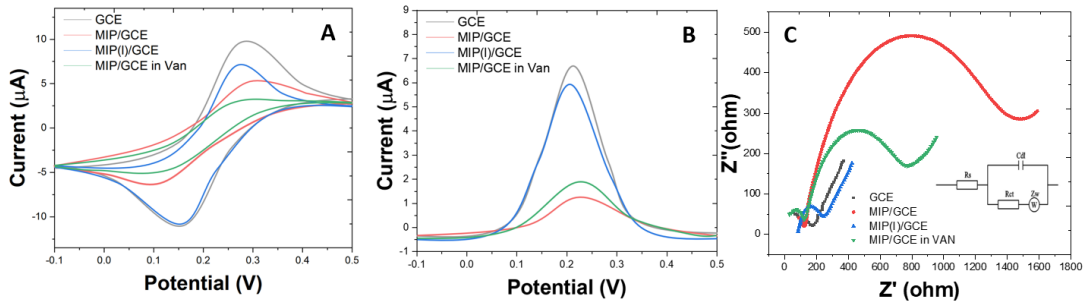

Figure 4. (A) CV, (B) DPV and (C) EIS curves of GCE, MIP/GCE, MIP(I)/GCE and MIP/GCE in VAN in 5 mM $[Fe(CN)_6]^{3-/4-}$ solution.

To maximize the electrochemical sensor's detection performance, parameters such as template elution time and re-recognition time were improved. VAN was extracted from the MIP using ethanol/acetic acid (V/V =95:5) as the eluent to create a cavity and improve the elution time. The change in current responsiveness during elution is depicted in Figure 5A. The response current value grew gradually as the elution duration increased, indicating that the template molecules were gradually eluted and the imprinting cavity expanded. Simultaneously, the $[Fe(CN)_6]^{3-/4-}$ electroactive probe reaches the electrode surface via the cavity, progressively increasing the response current. Similarly, after 20 minutes of elution, the peak current and impedance values attain equilibrium and tend to remain steady. As a result, the ideal elution time is 20 minutes. After electrochemical measurement, the electrode was submerged in water for 10 minutes and properly cleaned to remove leftover ethanol, acetic acid, and adsorption matrix.

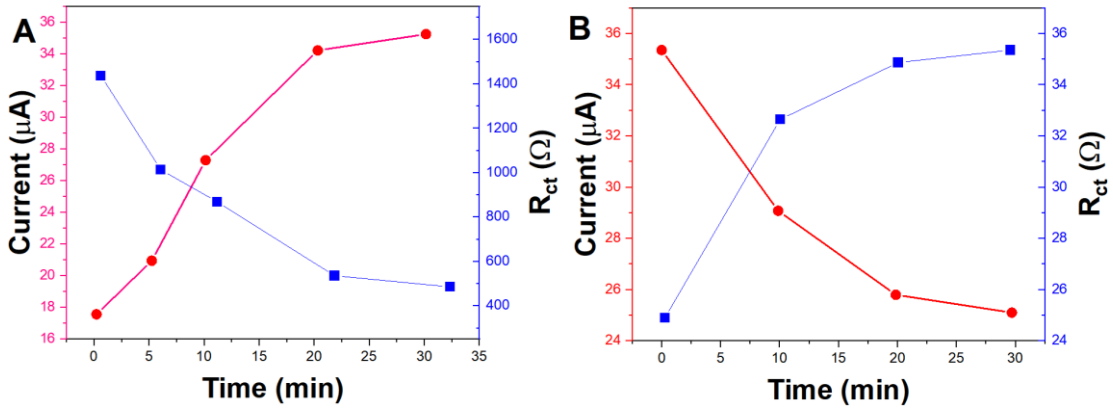

Figure 5. The influence of elution time (A) and re-identification time (B) on the response signal.

The time of re-recognition is an important basis for evaluating the performance of electrochemical sensors. The electrode was placed in 0.5 mM VAN to optimize the filling time of the imprinted cavity. After recognition, the electrode was thoroughly washed with water and electrochemical measurement was performed. Figure 5B shows the change of current response in the process of re-identification. As can be seen from the figure, the peak current value decreases gradually with the

increase of re-recognition time, indicating that the cavity is gradually occupied by template molecules [64,65]. Meanwhile, the amount of $[Fe(CN)_6]^{3-/4-}$ electrochemically active probes in contact with the electrode surface gradually decreased. Correspondingly, because the imprinted cavity is filled by the target molecule, the impedance increases gradually. When the recognition time is 20 min, the peak current and impedance reach equilibrium. Therefore, the optimal time for VAN re-recognition is 20 min.

To evaluate the response of the MIP/GCE sensor to the concentration of VAN, we recorded the electrochemical signal in the concentration range of VAN from 1×10^{-11}~1×10^{-4} M prepared in PBS under optimal conditions. We placed MIP/GCE in VAN solution for 20 min, and then measured its impedance response [66]. As shown in Figure 6A, the charge transfer resistance (R_{ct}) increases with the increase of VAN concentration. This is because VAN specifically binds to the holes of the imprinted polymer, preventing $[Fe(CN)_6]^{3-/4-}$ from reaching the electrode surface and increasing the impedance [67,68]. In addition, the increase of impedance response signal (ΔR_{ct}) is proportional to the logarithm of VAN concentration. As shown in Figure 6B, when VAN concentration is within the range of 1×10^{-11}-1×10^{-4} M, the ΔR_{ct} of MIP/GCE shows a good linear relationship with the calibration curve of lg_C, and the correlation coefficient R^2 is 0.989. The limit of detection can be calculated to be 5×10^{-12} M. Table 1 shows the analytical performance comparison with previous literature. It can be seen that the proposed MIP/GCE exhibited an excellent sensing performance compared with previous reports.

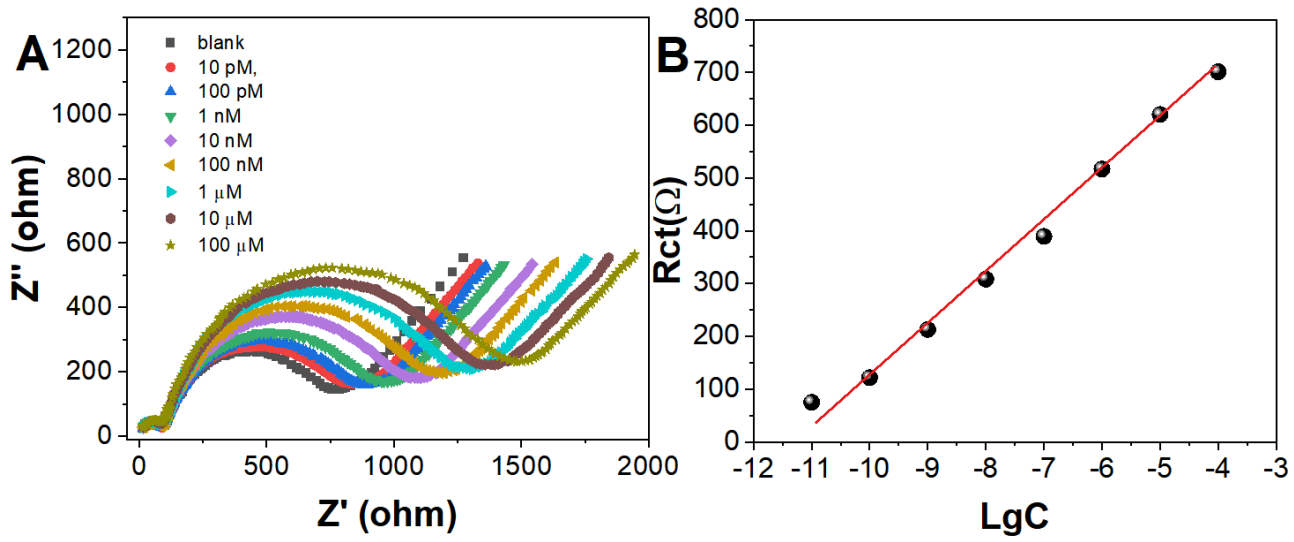

Figure 6. (A) Impedance response of the molecularly imprinted sensor towards 10 pM, 100 pM, 1 nM, 10 nM, 100 nM, 1 μM, 10 μM and 100 μM of VAN. (B) Plots of logarithm of VAN concentration against the Rct.

Several interfering substances including glucose (GLU), ascorbic acid (AA), uric acid (UA) and bisphenol A (BPA) were used to detect the VAN selectivity of MIP/GCE. Figure 7 shows the impedance response △Rct of each substance in electrochemical analysis. The larger ΔR_{ct} is, the higher the sensitivity of the sensor to the substance is. In order to prove that the prepared molecularly imprinted sensor has better selectivity for VAN molecules, the concentration of VAN was set at 10 nM, while the

concentration of other molecules was set at 100 nM. The impedance response of MIP/GCE to the template molecule VAN is the largest, although the interference concentration is much larger than the concentration of VAN [75]. For other interfering substances, the lack of specificity of molecularly imprinted cavity recognition will lead to non-specific binding and adsorption of other compounds, as well as large changes in electrical resistance, which limits the practical application of molecularly imprinted electrochemical sensors.

Table 1. Comparison of previously reported VAN electrochemical sensor with this work.

Electrode	Detection method	LR	LOD	Ref
Low-defect graphene electrodes	DPV	0.2 to 40 µM	10 nM	[69]
AgNP/graphene/GCE	SWV	2 to 100 µM	0.332 µM	[70]
AuNP-PAH/GCE	SWV	0.9 to 15 µM	0.055 µM	[71]
Ag-Pd	CV	0.02 to 45 µM	0.005 µM	[72]
MnO_2-GO	DPV	0.03 to 30 µM	0.0013 µM	[73]
Al-TiO_2-NPs	LSV	0.1 to 5 µM	0.02 µM	[74]
MIP/GCE	EIS	10 pM to 100 µM	5 pM	This work

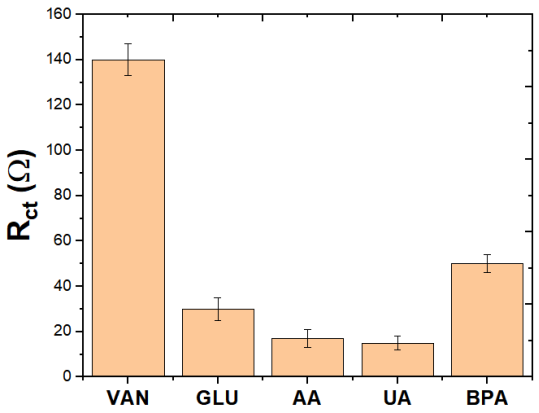

Figure 7. Response signals of VAN and other compounds on MIP/GCE (n=3)

The application feasibility of MIP/GCE was investigated using custard, milk tea and cake as real samples. Typically, 0.5 g sample was added into 50 mL ethanol under sonication for 30 min to obtain a homogeneous suspension. The suspension was centrifuged to collect the supernatant. Then, 1 mL of supernatant was added into 10 mL 5 mM $[Fe(CN)_6]^{3-/4-}$ solution for sensing. Table 2 showed the sensing results for three parallel detections. The results indicated that the content of VAN obtained from MIP/GCE has a good recovery. Therefore, the MIP/GCE showed excellent feasibility for VAN detection in food samples.

Table 2. Determination of VAN in custard, milk tea and cake (n = 3).

Sample	Found (μM)	Added (μM)	Total found (μM)	Recovery (%)
Custard	7.33	1.00	8.24	98.20
Milk tea	6.25	2.00	8.17	99.03
Candy	4.22	5.0	9.45	100.83

4. CONCLUSION

In this work, a specific method for VAN detection was constructed using molecular imprinting and electrochemical sensor. We found that ethanol/acetic acid (V/V =95:5) as the eluent had the best effect when the elution time was 20 min. The current decreases with the increase of VAN concentration (the impedance increases with the increase of VAN concentration), and the logarithm of the current decreases with the increase of VAN concentration, and the logarithm of the current decreases linearly with the increase of VAN concentration from 1.0×10^{-11} M to 1.0×10^{-4} M. However, due to the insufficient specificity of molecularly imprinted cavity recognition, VAN detection in complex matrix cannot be achieved. Therefore, we need to continue to explore a sensor with better anti-interference ability in future work to achieve more accurate detection of VAN in the presence of multiple interfering substances.

ACKNOWLEDGMENTS
This work was supported by (1) the Education Department of Henan Province (Project #20B530004); (2) Nanyang Science and Technology Bureau (Project #JCQY004); and (3) Nanyang Key Laboratory of Catalytic Functional Materials; (4) Interdisciplinary Sciences Project, Nanyang Institute of Technology

References

1. J. Yang, W. Feng, K. Liang, C. Chen, C. Cai, *Talanta*, 212 (2020) 120744.
2. L. Guo, H. Zheng, C. Zhang, L. Qu, L. Yu, *Talanta*, 210 (2020) 120621.
3. S. Ramanavicius, A. Jagminas, A. Ramanavicius, *Polymers*, 13 (2021) 974.
4. S. Motia, B. Bouchikhi, N. El Bari, *Talanta*, 223 (2021) 121689.
5. M. Harijan, V. Shukla, A.K. Singh, R. Raghuwanshi, G. Nath, M. Singh, *Biosensors and Bioelectronics: X*, 10 (2022) 100090.
6. T.C. Pereira, N.R. Stradiotto, *Microchimica Acta*, 186 (2019) 764.
7. S. Yang, Y. Teng, Q. Cao, C. Bai, Z. Fang, W. Xu, *Journal of The Electrochemical Society*, 166 (2019) B23.
8. M.A. Beluomini, J.L. da Silva, A.C. de Sá, E. Buffon, T.C. Pereira, N.R. Stradiotto, *Journal of Electroanalytical Chemistry*, 840 (2019) 343.
9. I. Seguro, J.G. Pacheco, C. Delerue-Matos, *Sensors*, 21 (2021) 1975.
10. Y. Yang, W. Yan, C. Guo, J. Zhang, L. Yu, G. Zhang, X. Wang, G. Fang, D. Sun, *Analytica Chimica Acta*, 1106 (2020) 1.
11. P. Tong, Y. Meng, J. Liang, J. Li, *Sensors and Actuators B: Chemical*, 330 (2021) 129405.
12. Y. Saylan, S. Akgönüllü, H. Yavuz, S. Ünal, A. Denizli, *Sensors*, 19 (2019) 1279.

13. H. Karimi-Maleh, A. Ayati, R. Davoodi, B. Tanhaei, F. Karimi, S. Malekmohammadi, Y. Orooji, L. Fu, M. Sillanpää, *Journal of Cleaner Production*, 291 (2021) 125880.
14. L. Fu, X. Zhang, S. Ding, F. Chen, Y. Lv, H. Zhang, S. Zhao, *Current Pharmaceutical Analysis*, 18 (2022) 4.
15. P. Rebelo, E. Costa-Rama, I. Seguro, J.G. Pacheco, H.P.A. Nouws, M.N.D.S. Cordeiro, C. Delerue-Matos, *Biosensors and Bioelectronics*, 172 (2021) 112719.
16. A.G. Ayankojo, J. Reut, V. Ciocan, A. Öpik, V. Syritski, *Talanta*, 209 (2020) 120502.
17. N. Hareesha, J.G. Manjunatha, B.M. Amrutha, N. Sreeharsha, S.M. Basheeruddin Asdaq, Md.K. Anwer, *Colloids and Surfaces A: Physicochemical and Engineering Aspects*, 626 (2021) 127042.
18. L. Fu, K. Xie, D. Wu, A. Wang, H. Zhang, Z. Ji, *Materials Chemistry and Physics*, 242 (2020) 122462.
19. M. Qianwen, D. Yaping, L. Li, W. Anqing, D. Dingding, Z. Yijun, *Journal of Electroanalytical Chemistry*, 833 (2019) 297.
20. Y. Tian, P. Deng, Y. Wu, J. Liu, J. Li, G. Li, Q. He, *Microchemical Journal*, 157 (2020) 104885.
21. Y. Sun, X. Jiang, H. Jin, R. Gui, *Analytica Chimica Acta*, 1083 (2019) 101.
22. H. Karimi-Maleh, Y. Orooji, F. Karimi, M. Alizadeh, M. Baghayeri, J. Rouhi, S. Tajik, H. Beitollahi, S. Agarwal, V.K. Gupta, *Biosensors and Bioelectronics* (2021) 113252.
23. H. Karimi-Maleh, A. Khataee, F. Karimi, M. Baghayeri, L. Fu, J. Rouhi, C. Karaman, O. Karaman, R. Boukherroub, *Chemosphere* (2021) 132928.
24. J. Li, S. Zhang, L. Zhang, Y. Zhang, H. Zhang, C. Zhang, X. Xuan, M. Wang, J. Zhang, Y. Yuan, *Frontiers in Chemistry*, 9 (2021) 339.
25. Z. Wu, J. Liu, M. Liang, H. Zheng, C. Zhu, Y. Wang, *Frontiers in Chemistry*, 9 (2021) 208.
26. Y. Zheng, D. Wang, X. Li, Z. Wang, Q. Zhou, L. Fu, Y. Yin, D. Creech, *Biosensors*, 11 (2021) 403.
27. D. Wang, D. Li, L. Fu, Y. Zheng, Y. Gu, F. Chen, S. Zhao, *Sensors*, 21 (2021) 8216.
28. K. Murtada, V. Moreno, *Journal of Electroanalytical Chemistry*, 861 (2020) 113988.
29. J. Zhou, Y. Zheng, J. Zhang, H. Karimi-Maleh, Y. Xu, Q. Zhou, L. Fu, W. Wu, *Null*, 53 (2020) 2517.
30. L. Fu, A. Yu, G. Lai, *Chemosensors*, 9 (2021) 282.
31. Y. Wang, L. Chen, T. Xuan, J. Wang, X. Wang, *Frontiers in Chemistry*, 9 (2021) 569.
32. H. Karimi-Maleh, F. Karimi, L. Fu, A.L. Sanati, M. Alizadeh, C. Karaman, Y. Orooji, *Journal of Hazardous Materials*, 423 (2022) 127058.
33. H. Karimi-Maleh, M. Alizadeh, Y. Orooji, F. Karimi, M. Baghayeri, J. Rouhi, S. Tajik, H. Beitollahi, S. Agarwal, V.K. Gupta, S. Rajendran, S. Rostamnia, L. Fu, F. Saberi-Movahed, S. Malekmohammadi, *Ind. Eng. Chem. Res.*, 60 (2021) 816.
34. H.D. Madhuchandra, B.E.K. Swamy, *Materials Science for Energy Technologies*, 2 (2019) 697.
35. L. Fu, Y. Zheng, A. Wang, P. Zhang, S. Ding, W. Wu, Q. Zhou, F. Chen, S. Zhao, *Journal of Herbal Medicine*, 30 (2021) 100512.
36. M. Chen, H. Yang, Z. Song, Y. Gu, Y. Zheng, J. Zhu, A. Wang, L. Fu, *Phyton-International of Experimental Botany*, 90 (2021) 1507.
37. W. Li, W. Luo, M. Li, L. Chen, L. Chen, H. Guan, M. Yu, *Frontiers in Chemistry*, 9 (2021) 610.
38. H. Karimi-Maleh, C. Karaman, O. Karaman, F. Karimi, Y. Vasseghian, L. Fu, M. Baghayeri, J. Rouhi, P. Senthil Kumar, P.-L. Show, S. Rajendran, A.L. Sanati, A. Mirabi, *Journal of Nanostructure in Chemistry* (2022) in-press.
39. H. Karimi-Maleh, A. Ayati, S. Ghanbari, Y. Orooji, B. Tanhaei, F. Karimi, M. Alizadeh, J. Rouhi, L. Fu, M. Sillanpää, *Journal of Molecular Liquids*, 329 (2021) 115062.

40. O.S. Ahmad, T.S. Bedwell, C. Esen, A. Garcia-Cruz, S.A. Piletsky, *Trends in Biotechnology*, 37 (2019) 294.
41. S. Kadirsoy, N. Atar, M.L. Yola, *New J. Chem.*, 44 (2020) 6524.
42. J.L. da Silva, E. Buffon, M.A. Beluomini, L.A. Pradela-Filho, D.A. Gouveia Araújo, A.L. Santos, R.M. Takeuchi, N.R. Stradiotto, *Analytica Chimica Acta*, 1143 (2021) 53.
43. N. Nontawong, M. Amatatongchai, P. Jarujamrus, D. Nacapricha, P.A. Lieberzeit, *Sensors and Actuators B: Chemical*, 334 (2021) 129636.
44. X. Wei, H. Chen, *Analytical and Bioanalytical Chemistry*, 411 (2019) 5809–5816.
45. A.A. Lahcen, A. Amine, *Electroanalysis*, 31 (2019) 188.
46. R.D. Crapnell, A. Hudson, C.W. Foster, K. Eersels, B. van Grinsven, T.J. Cleij, C.E. Banks, M. Peeters, *Sensors*, 19 (2019) 1204.
47. Y. Sun, H. Gao, L. Xu, G.I.N. Waterhouse, H. Zhang, X. Qiao, Z. Xu, *Food Chemistry*, 332 (2020) 127376.
48. F. Cui, Z. Zhou, H.S. Zhou, *Sensors*, 20 (2020) 996.
49. M. Amatatongchai, W. Sroysee, P. Sodkrathok, N. Kesangam, S. Chairam, P. Jarujamrus, *Analytica Chimica Acta*, 1076 (2019) 64.
50. K. Fu, R. Zhang, J. He, H. Bai, G. Zhang, *Biosensors and Bioelectronics*, 143 (2019) 111636.
51. C. Dong, H. Shi, Y. Han, Y. Yang, R. Wang, J. Men, *European Polymer Journal*, 145 (2021) 110231.
52. G. Tigari, J.G. Manjunatha, E.S. D'Souza, N. Sreeharsha, *ChemistrySelect*, 6 (2021) 2700.
53. T. Zabihpour, S.-A. Shahidi, H. Karimi-Maleh, A. Ghorbani-HasanSaraei, *Journal of Food Measurement and Characterization*, 14 (2020) 1039.
54. C. Raril, J.G. Manjunatha, *Microchemical Journal*, 154 (2020) 104575.
55. K. Chetankumar, B.E.K. Swamy, T.S.S.K. Naik, *Chemical Data Collections*, 28 (2020) 100392.
56. T. Dodevska, I. Vasileva, P. Denev, D. Karashanova, B. Georgieva, D. Kovacheva, N. Yantcheva, A. Slavov, *Materials Chemistry and Physics*, 231 (2019) 335.
57. A.B. Monnappa, J.G.G. Manjunatha, A.S. Bhatt, H. Nagarajappa, *Journal of Science: Advanced Materials and Devices*, 6 (2021) 415.
58. H.K.S.V. Mohan, W.K. Chee, Y. Li, S. Nayak, C.L. Poh, A.V.Y. Thean, *Materials & Design*, 186 (2020) 108208.
59. A. Venkadesh, J. Mathiyarasu, S. Radhakrishnan, *Materials Today Chemistry*, 22 (2021) 100554.
60. X. Nie, R. Zhang, Z. Tang, H. Wang, P. Deng, Y. Tang, *Nanomaterials*, 10 (2020) 1356.
61. V. Erady, R.J. Mascarenhas, A.K. Satpati, *Sensors International*, 1 (2020) 100023.
62. G. Tigari, J. Manjunatha, *Monatshefte Für Chemie-Chemical Monthly*, 151 (2020) 1681.
63. G. Ziyatdinova, A. Zhupanova, R. Davletshin, *Sensors*, 22 (2022) 288.
64. M. Kutty, R. Settu, S.-M. Chen, T.-W. Chen, T.-W. Tseng, A.A. Hatamleh, J. Yu, R. Yu, C.-C. Huang, *International Journal of Electrochemical Science*, 14 (2019) 5972.
65. M. Dong, S. Zhao, Y. Lv, F. Chen, A. Wang, L. Fu, C.-T. Lin, *Journal of Food Measurement and Characterization*, 15 (2021) 4718.
66. L. Taouri, M. Bourouina, S. Bourouina-Bacha, D. Hauchard, *Journal of Food Composition and Analysis*, 100 (2021) 103811.
67. A. Zhupanova, G. Ziyatdinova, *Chemistry Proceedings*, 5 (2021) 47.
68. E. Murugan, A. Dhamodharan, *Diamond and Related Materials*, 120 (2021) 108684.
69. M.-J. Song, S.W. Hwang, D. Whang, *Talanta*, 80 (2010) 1648.
70. L. Huang, K. Hou, X. Jia, H. Pan, M. Du, *Mater Sci Eng C Mater Biol Appl*, 38 (2014) 39.
71. T.R. Silva, D. Brondani, E. Zapp, I. Cruz Vieira, *Electroanalysis*, 27 (2015) 465.
72. J. Li, H. Feng, J. Li, J. Jiang, Y. Feng, L. He, D. Qian, *Electrochimica Acta*, 176 (2015) 827.
73. T. Gan, Z. Shi, Y. Deng, J. Sun, H. Wang, *Electrochimica Acta*, 147 (2014) 157.

74. K. Murtada, S. Jodeh, M. Zougagh, Á. Ríos, *Electroanalysis*, 30 (2018) 969.
75. M. Burç, Ö. Güngör, S. TİTRETİR DURAN, *Analytical and Bioanalytical Electrochemistry*, 12 (2020) 625.